Intrinsic electrocatalytic activity of nitrogen-doped monolayer graphene observed using a Janus bilayer design

Gloria Alexander[1], Tobias Grosser[1], Cathy Sulaiman[2], Raquel Sánchez-Barquilla[2], Emil Fuhry[1], Isabell Wachta[1], Robert Jungnickel[1], Jan Ingo Flege[2], Kannan Balasubramanian*[1]

[1] Department of Chemistry and School of Analytical Sciences Adlershof (SALSA), Humboldt-Universität zu Berlin, Germany

[2] Chair of Applied Physics and Semiconductor Spectroscopy, Brandenburg University of Technology Cottbus-Senftenberg, 03046 Cottbus, Germany

**Corresponding author e-mail: nano.anchem@hu-berlin.de*

SUPPLEMENTARY INFORMATION

Figure S1. (a) Optical image of an SiO_2/Si substrate patterned with Pt electrode lines. The presence of the transferred SLG is discernible by its optical contrast relative to the bare SiO_2/Si regions. (b) Optical image after the second transfer step showing the polystyrene (PS)/N-BLG stack on the same wafer. The PS/N-BLG layer covers nearly the entire SLG area, indicating a nearly complete coverage of the underlying SLG by the transferred PS/N-BLG layer. Prior to electrochemical measurements, the PS coating is removed in toluene.
There is only a small fraction of the N-doped sheet extending beyond the bottom SLG or vice versa. Therefore, we do not expect those areas to affect the overall electrochemical response of the N-BLG electrode.

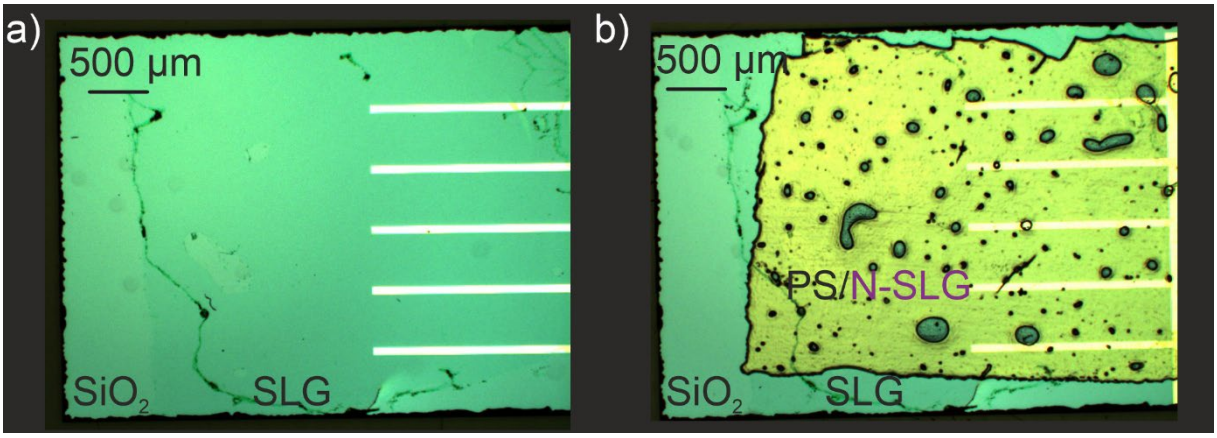

Figure S2. Electrochemical etching (e-etching) of bilayer graphene electrodes. Cyclic voltammetry in 100 mM HCl was employed to remove residual trace metal impurities (mainly copper) from the transferred graphene layers, following the procedure reported by Iost et al. [1] The arrows indicate the oxidation of copper and its removal during the continuous cycling.

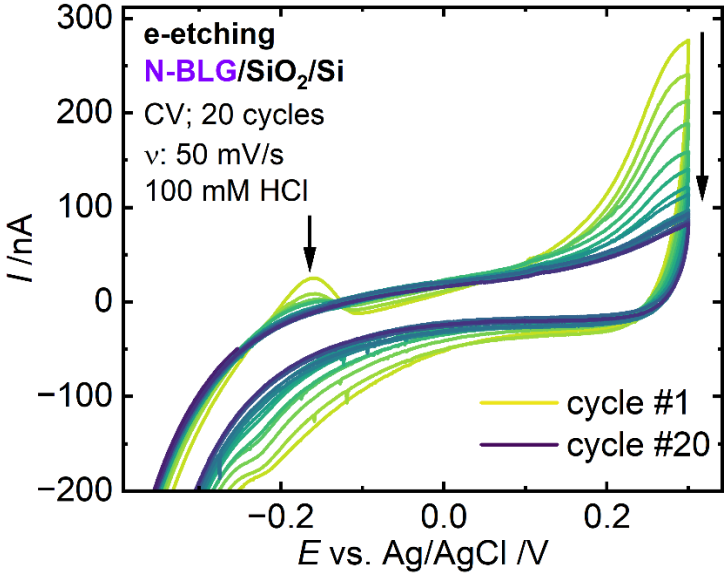

Figure S3. (a) AFM height image of a typical SLG. (b) Height profile along the blue line shown in (a), indicating a step height of ~1.5 nm, consistent with a single graphene sheet supported on SiO_2/Si.

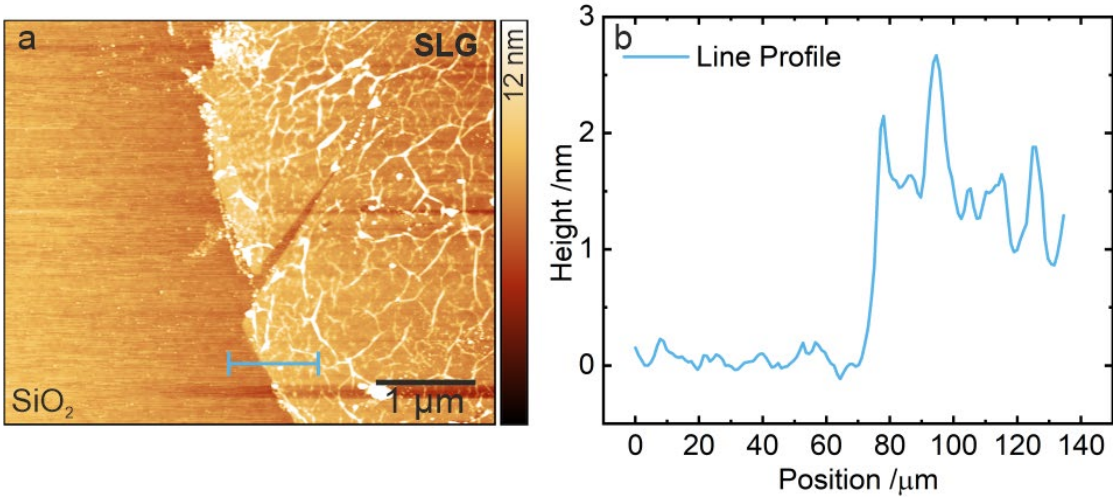

Figure S4. Water contact angles measured on (a) pristine BLG and (b) N-BLG. The contact angle decreases from ~69° (BLG) to ~58° (N-BLG), indicating an increased hydrophilicity of the graphene surface after nitrogen plasma treatment.

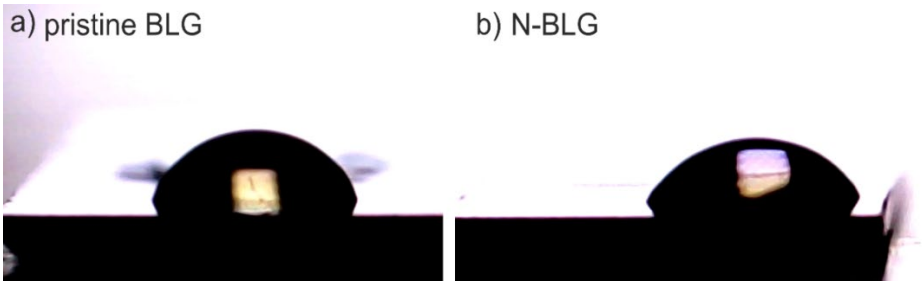

Figure S5. Zoom-in of the Raman spectra presented in Figure 2(c) showing a close-up of the *2D* band region.

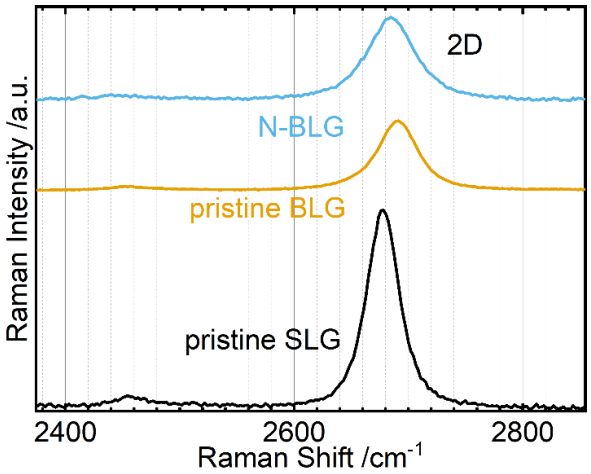

Figure S6. XPS survey spectrum on N-SLG (on copper foil) prepared by plasma treatment in nitrogen for 6 s. The assignment of peaks is based on literature values. [2]

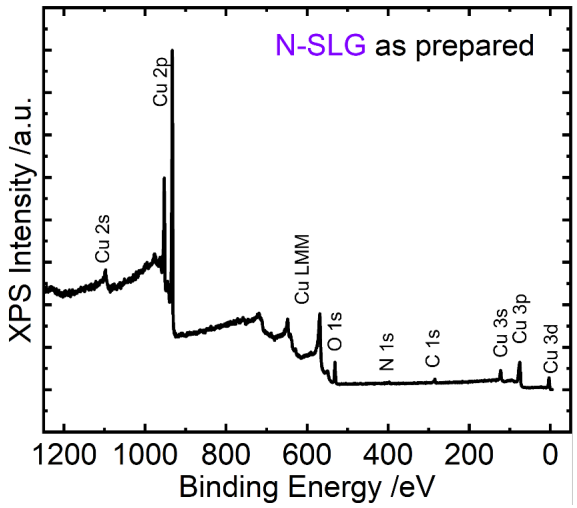

Detailed XPS analysis

Figure S7 presents a direct comparison of high resolution XPS spectra obtained on pristine SLG with that recorded on N-SLG. As discussed in main text, we fit the C 1s spectrum of pristine SLG (Figure S7a) mainly with sp^2 and sp^3 components. This is consistent with XPS spectra reported in our previous works, [3, 4] where we have shown that, even after transfer, we have negligible proportion of oxygen-containing groups on pristine graphene. By fitting an additional peak at 288.6 eV, we can, in principle, obtain a negligibly small contribution (marked as # in Figure S7a), which could be attributed to C=O. It is apparent that we do not have evidence for the presence of other components such as C-O or O-C=O in the C 1s spectrum. The N 1s spectrum in Figure S7b confirms the absence of nitrogen-containing groups in pristine graphene.

On N-SLG, we assign the additional peak in the C 1s spectrum (Figure S7c) to C-N. In principle, based solely on the C 1s spectra, it is difficult to definitively exclude oxygen-containing groups, since the C=O peak lies very close (binding energy difference < 0.3 eV) to the C-N peak. The assignment of C-N in the C 1s spectrum is supported by the evidence from the N 1s spectra (Figure S7d). On pristine SLG, we do not observe any signal in the N 1s region, whereas on N-SLG, we obtain a very clear, asymmetric N 1s peak profile. Moreover, we ensure that oxygen contamination in the plasma chamber is limited only to trace amounts. Further support for the limited incorporation of oxygen groups comes from the absence of additional peaks in the C 1s spectra (related to C-O and O-C=O), as typically reported for graphene modified with oxygen plasma. [5-7]

Figure S7. Comparison of XPS spectra of (a,b) pristine single layer graphene (SLG) with that of (c,d) nitrogen-doped graphene (N-SLG), the latter prepared by gentle nitrogen plasma treatment for 6 s. (a,c) High resolution C 1s and (b,d) high resolution N 1s spectra.

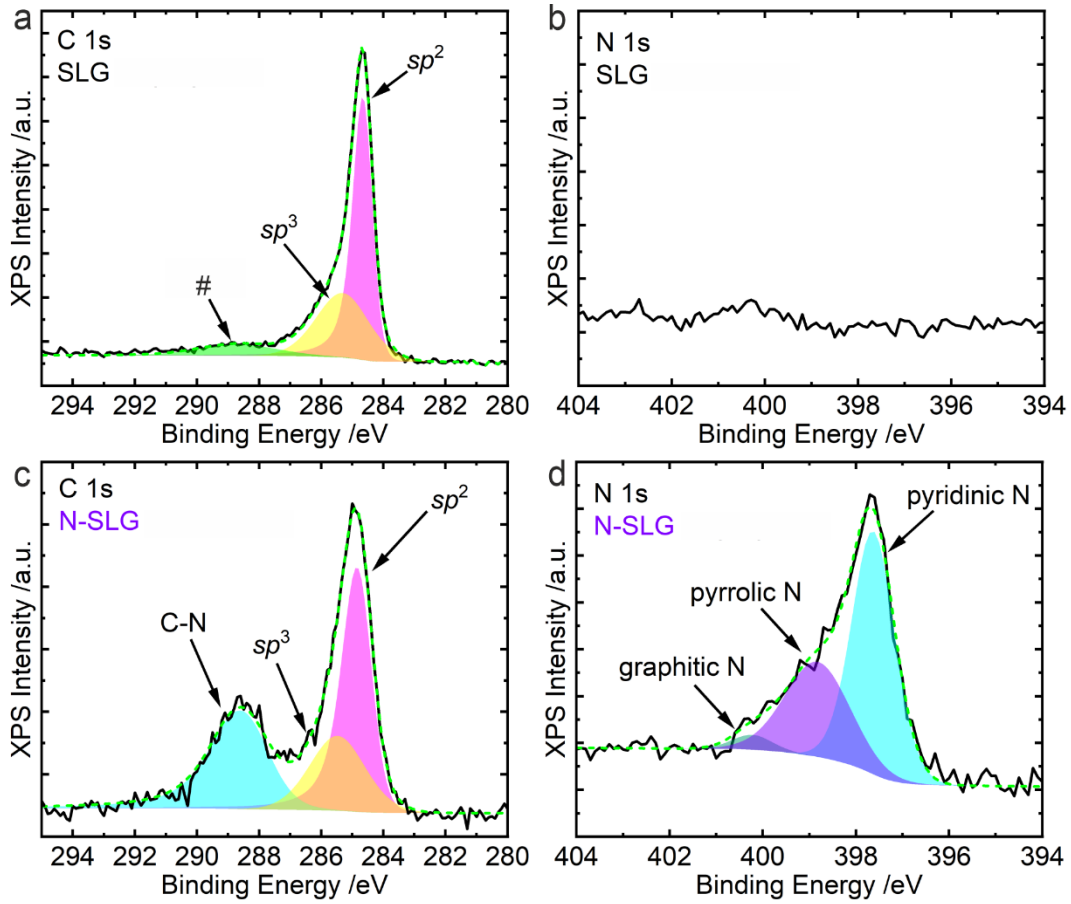

Figure S8. XPS spectra of N-SLG measured four days after preparation. (a) High resolution C 1s spectrum showing the dominant sp^2 and minor sp^3 contributions with a persistent C-N signal – very similar to the as-prepared sample (Figure 3). (b) High resolution N 1s spectrum deconvoluted into the two main components, pyridinic N (~397.6 eV; ~49 %), and pyrrolic N (~398.8 eV; ~50 %). The graphitic N component appears to be almost negligible (< 2%). Compared to the as-prepared sample (Figure 3), these data indicate a modest redistribution of nitrogen species during ambient aging. See Table S1 for quantitative details.

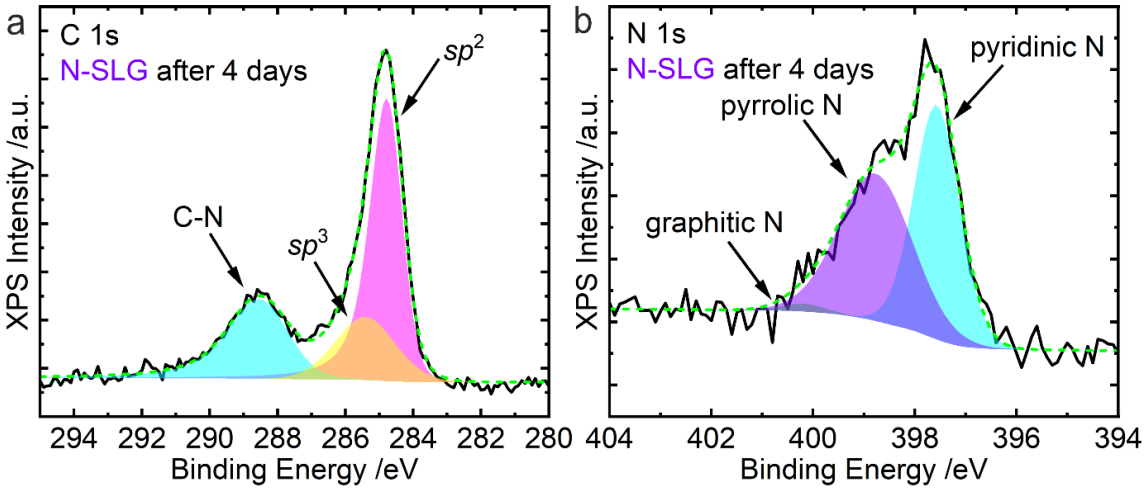

Table S1: Evolution of N 1s XPS peak composition of nitrogen-doped graphene (N-SLG) immediately after preparation and after four days. Percentages are calculated as the area of each component relative to the total N 1s envelope.

Component	As prepared area	As prepared percentage	After 4 days area	After 4 days percentage	Change in %
Pyridinic N	306.2	60.7 %	212.2	48.8 %	-11.9 %
Pyrrolic N	180.7	35.8 %	215.5	49.6 %	+13.8 %
Graphitic N	17.3	3.4 %	6.8	1.6 %	-1.8 %

Figure S9. CV of an SLG electrode (on SiO_2/Si) recorded with 1 mM $FeCN_6$ in buffers of pH 3, 5, and 7. The data show a pH-dependent shift of the redox peaks and an increased peak-to-peak separation indicating slower ET kinetics at higher pH. [3]

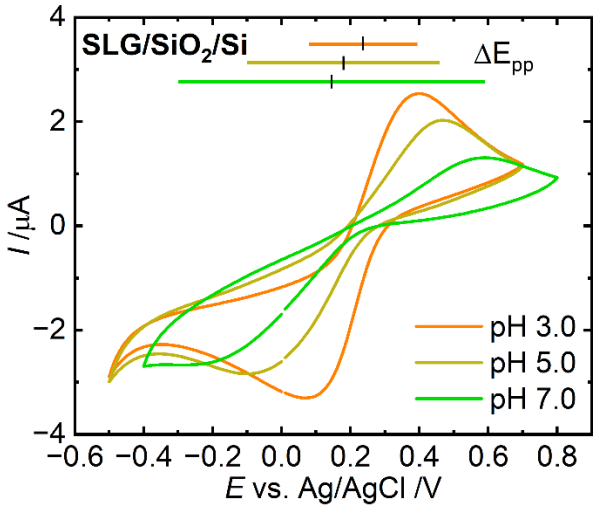

Figure S10. CVs of the cationic probe 1 mM hexaammineruthenium(III) chloride (HARu) recorded in buffers of pH 3, 5 and pH 7. Scan rate: 50 mV/s. (a) Pristine BLG shows pH-dependent variations in peak-to-peak separation and current response. (b) N-BLG exhibits nearly overlapping redox peaks and a constant peak-to-peak separation, confirming a pH-independent and reversible ET behavior for this cationic redox probe.

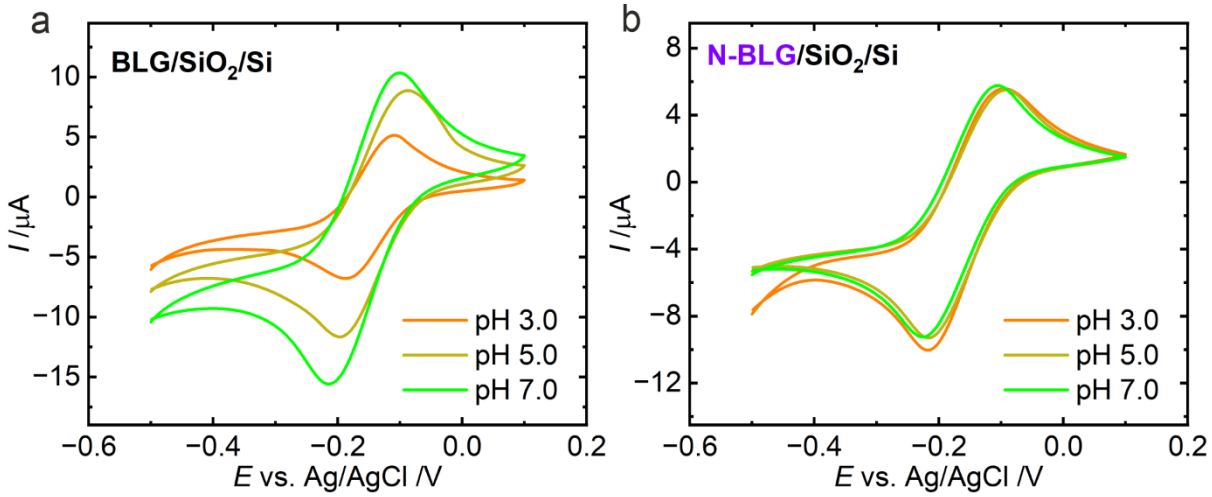

Electrochemical Impedance Spectroscopy of pristine BLG and N-BLG

We have utilized Electrochemical Impedance Spectroscopy (EIS) to characterize the interface of pristine BLG and N-BLG electrodes. To gather information about the electron transfer kinetics, we have acquired EIS data in a solution of ferricyanide in a buffer of pH 7, as shown in Figure S11. The EIS data were acquired in a frequency range of 50 mHz – 2 kHz and were fit using a Randles equivalent circuit, comprised of a series resistance R_1, a constant phase element modeling the double layer (Q_{EDL}), a charge transfer resistance (R_{ct}) signifying the electron transfer with ferricyanide and a Warburg element (W, Warburg coefficient A_W) characterizing the diffusion of the redox active species towards the electrode. R_1 comprises of both the solution resistance and the series resistance of the graphene electrode. The impedance of Q_{EDL} (Z_Q) is given by $Z_Q^{-1} = C_\alpha (j\,\omega)^\alpha$, where C_α is the non-ideal capacitance and α is the order. α is a measure of the non-ideality of the capacitance in the range of $0 < \alpha \leq 1$. It is apparent that we obtain a considerably good fit with the proposed equivalent circuit.

Table S2 collects the results of the fitting showing the parameters and errors in the fit. The charge transfer resistance (R_{ct}) on pristine BLG is estimated to be 383.8 kΩ, while it is only 12.9 kΩ on N-BLG, which is more than an order of magnitude lower. This implies a significant improvement in electron transfer kinetics with ferricyanide on N-BLG, consistent with the CV measurements in different buffer solutions. The series resistance R_1 is found to increase on N-BLG. This can be understood by considering that after plasma treatment the sp^2-carbon framework is modified implying an increase in resistance. The capacitance values are similar for both cases. For the EIS data of pristine BLG (Figure S11a), no distinct Warburg contribution is observed in the investigated frequency range. This indicates that poor electron transfer kinetics at the pristine BLG electrode dominate the impedance response.

Figure S11. Nyquist plots of electrochemical impedance spectra acquired on (a) pristine BLG and (b) N-BLG obtained in a solution of 1 mM ferricyanide in pH 7 measured at the formal potential of the redox species in solution. The measured data (black squares) are fit (blue line) with an equivalent circuit indicated in the inset of the graphs. The results of the fitting are presented in table S2. R_1 – series resistance (solution + graphene), Q_{EDL} – non-ideal capacitance, R_{ct} – charge transfer resistance, W – Warburg element. See text above for further details.

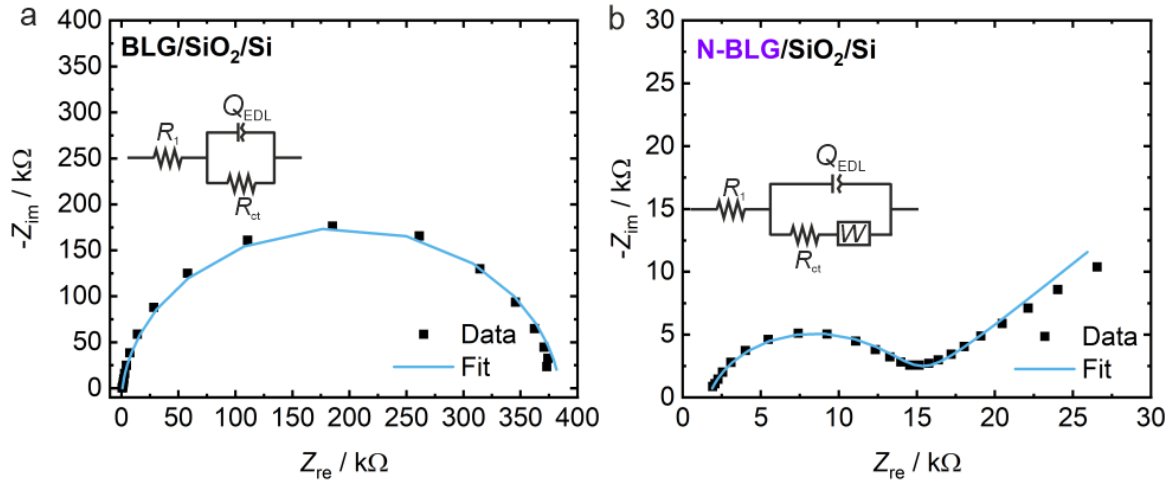

Table S2: Parameter values obtained for the fit of the data shown in Figure S11. The data are fit by using the Randles equivalent circuit shown in the corresponding inset of Figure S11. See text above for details of parameters. It is apparent that the charge transfer resistance R_{ct} is smaller by more than one order of magnitude on N-BLG signifying improved electron transfer kinetics on N-BLG.

a) Fit parameters for the ***pristine BLG*** electrode using the data shown in Figure S11a.

Parameter	Value	Fit Error in %
R_1	0.8291 kΩ	4.07 %
R_{ct}	383.8 kΩ	2.27 %
C_α	4.121 x 10^{-7} $F \cdot s^{(\alpha-1)}$	3.86 %
α	0.9378	0.72 %

b) Fit parameters for the ***N-BLG*** electrode using the data shown in Figure S11b.

Parameter	Value	Fit Error in %
R_1	1.638 kΩ	3.19 %
R_{ct}	12.9 kΩ	1.67 %
A_W	1.095 x 10^{-4} Ω· $s^{-1/2}$	3.16 %
C_α	5.103 x 10^{-7} $F \cdot s^{(\alpha-1)}$	8.90 %
α	0.8301	1.56 %

Figure S12. CV of an N-BLG electrode (on SiO_2/Si) recorded in blank buffer of pH 7.

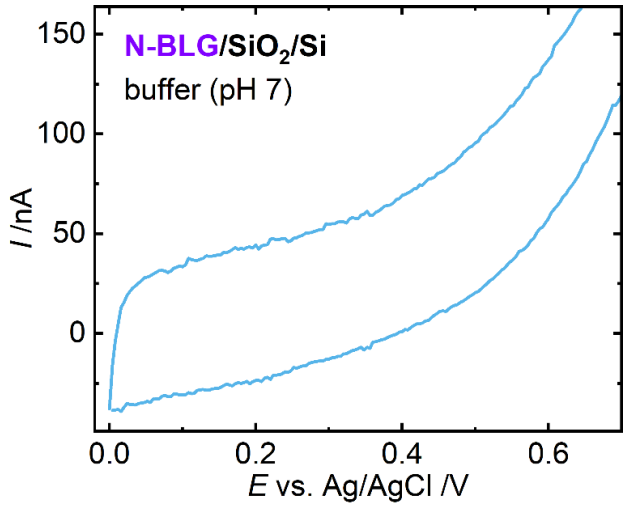

Figure S13. (a) CVs of 100 consecutive cycles measured at an N-BLG electrode in 1 mM NADH (pH 7) at a scan rate of 50 mV/s. (b) CVs of 1 mM 1,1'-ferrocendimethanol (FDM, 100 mM KCl, scan rate 50 mV/s) recorded before and after NADH cycling, showing almost identical responses and no discernible changes in peak positions or currents. These data confirm the robustness of the N-BLG electrode under continuous electrochemical cycling. (c) Raman spectra of N-BLG recorded before and after NADH cycling. The spectra show negligible differences, indicating that the structural integrity of the N-BLG electrode is maintained.

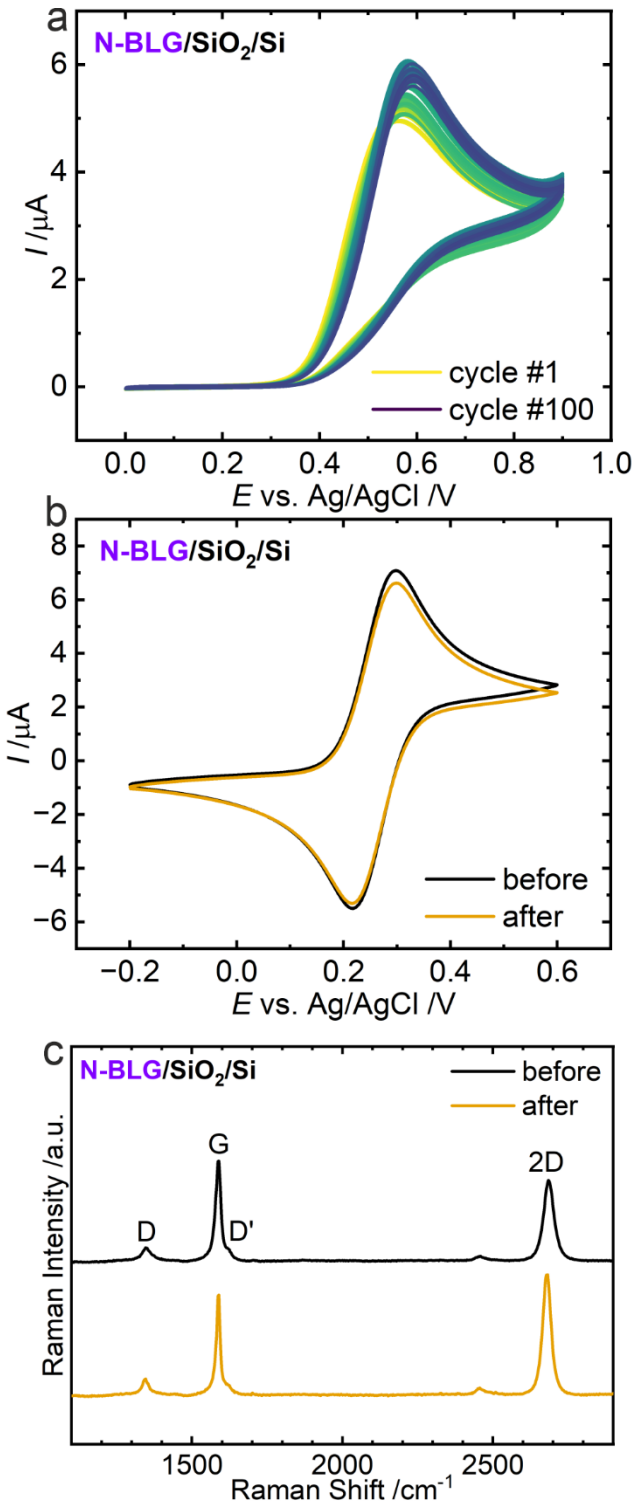

Figure S14. Effect of longer N_2 plasma exposure on NADH electrocatalysis and graphene structure. (a) CVs of 1 mM NADH (pH 7) for N-BLG prepared with 0 s, 9 s, and 12 s plasma exposure at a scan rate of 50 mV/s. The 9 s sample shows the lowest onset potential, whereas the 12 s sample exhibits a higher onset potential and a broadened oxidation peak, indicating a diminished electrocatalytic activity after prolonged plasma treatment. (b) Raman spectra of pristine BLG and N-BLG after a 12 s plasma exposure. The latter shows strongly reduced intensity and pronounced broadening of the D, G, and 2D bands. This is consistent with a substantial plasma-induced disorder and structural degradation of the graphene lattice.

It is worth mentioning that we still see a sizeable current and graphene-related Raman peaks, since the bottom layer is still pristine graphene.

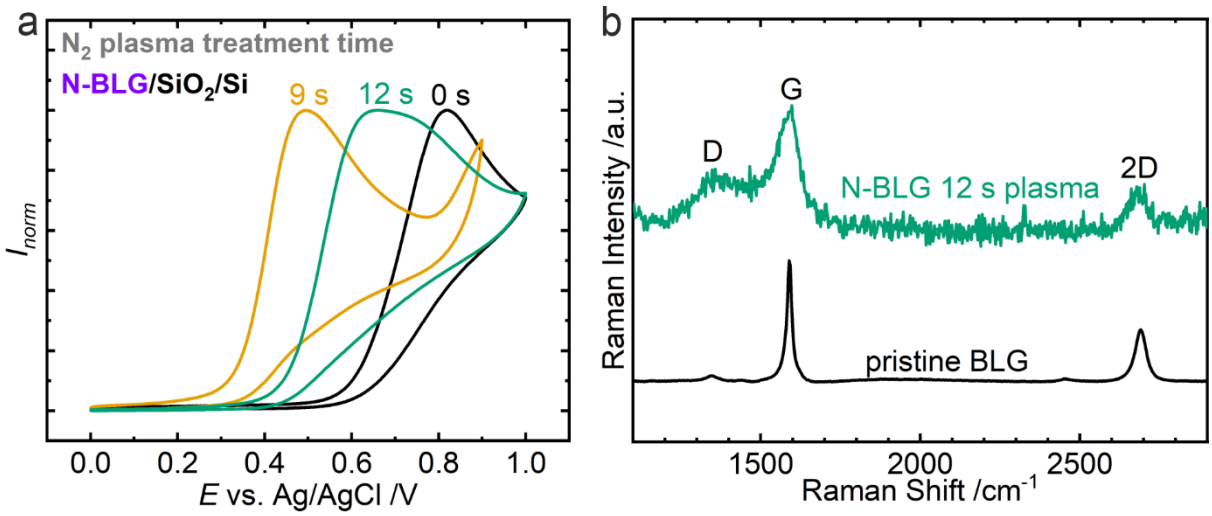

Figure S15. Evaluation of ORR at the fabricated electrodes. CVs of (a) a pristine BLG and (b) a N-BLG electrode in saturated N_2 and O_2 in 0.1 M $HClO_4$. Scan rate: 50 mV/s. (c) Direct comparison of the corresponding background-subtracted CVs in O_2 atmosphere showing a comparatively lower overpotential for ORR at the N-BLG electrode.

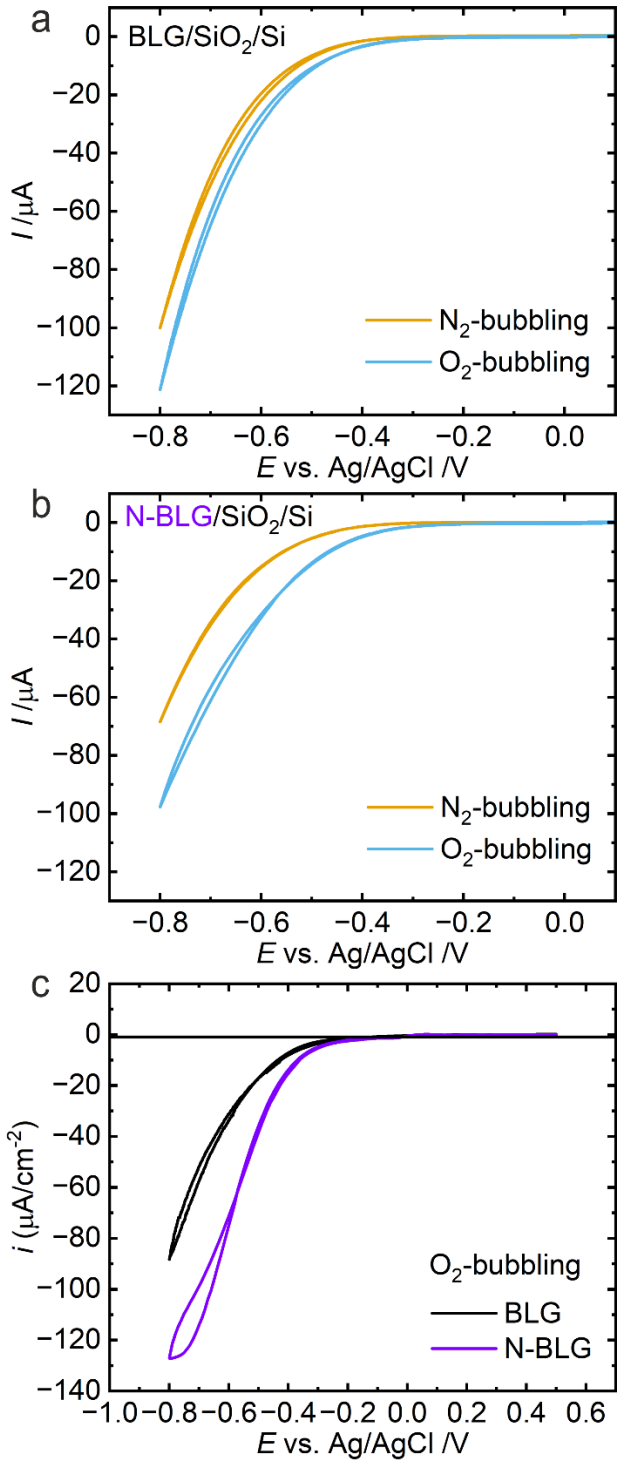

SUPPLEMENTARY REFERENCES

1. R. M. Iost, F. N. Crespilho, L. Zuccaro, H. K. Yu, A. M. Wodtke, K. Kern and K. Balasubramanian, Enhancing the Electrochemical and Electronic Performance of CVD-Grown Graphene by Minimizing Trace Metal Impurities, *ChemElectroChem*, 2014, **1**, 2070-2074.
2. J. F. Moulder, W. F. Stickle, P. E. Sobol and K. D. Bomben, *Handbook of X-ray Photoelectron Spectroscopy*, Perkin-Elmer Corporation, 1992.
3. M. Wehrhold, T. J. Neubert, A. Yadav, M. Vondracek, R. M. Iost, J. Honolka and K. Balasubramanian, pH sensitivity of interfacial electron transfer at a supported graphene monolayer, *Nanoscale*, 2019, **11**, 14742-14756.
4. M. Wehrhold, T. J. Neubert, T. Grosser, M. Vondracek, J. Honolka and K. Balasubramanian, A highly durable graphene monolayer electrode under long-term hydrogen evolution cycling, *Chem Commun (Camb)*, 2022, **58**, 3823-3826.
5. F. Hadish, S. Jou, B.-R. Huang, H.-A. Kuo and C.-W. Tu, Functionalization of CVD Grown Graphene with Downstream Oxygen Plasma Treatment for Glucose Sensors, *J. Electrochem. Soc.*, 2017, **164**, B336.
6. R. Lukose, M. Lisker, F. Akhtar, M. Fraschke, T. Grabolla, A. Mai and M. Lukosius, Influence of plasma treatment on SiO2/Si and Si3N4/Si substrates for large-scale transfer of graphene, *Sci. Rep.*, 2021, **11**, 13111.
7. Y.-k. Niu, K.-x. Bi, Q.-n. Li, S.-y. Zhou, J.-l. Mu, L.-g. Tan and L.-y. Mei, Optical Study of Few-Layer Graphene Treated by Oxygen Plasma, *physica status solidi (b)*, 2022, **259**, 2200197.